

# High-Performance All-Solid-State Dye-Sensitized Solar Cells Utilizing Imidazolium-Type Ionic Crystal as Charge Transfer Layer

Yong Zhao,<sup>†,‡</sup> Jin Zhai,<sup>\*,†,‡</sup> Jinling He,<sup>†,‡</sup> Xiao Chen,<sup>†,‡</sup> Li Chen,<sup>†,‡</sup> Libing Zhang,<sup>†</sup>  
Yuxi Tian,<sup>†,‡</sup> Lei Jiang,<sup>†</sup> and Daoben Zhu<sup>†</sup>

Beijing National Laboratory for Molecular Sciences (BNLMS), Center for Molecular Science, Institute of Chemistry, and Graduate University of the Chinese Academy of Sciences, Beijing 100080, China

Received March 7, 2008. Revised Manuscript Received June 9, 2008

An organic ionic crystal, 1-methyl-3-acetyl-imidazolium iodide (MA-II), was synthesized and applied into all-solid-state dye-sensitized solar cells as electrolyte material. We adopted 1-methyl-3-propylimidazolium tetra-fluoroborate as a crystal growth inhibitor, lithium bis-trifluoro-methanesulfonylimide as a charge transport enhancer, and 4-*tert*-butyl pyridine as a carrier recombination inhibitor. The solar cell devices achieved the total conversion efficiencies of 2.6 and 2.0% under half a sun and one sun irradiation, respectively, showing a good stability even without any sealing and protection from ambient condition. The inner work mechanism of solar cell devices was analyzed by measuring the photovoltage, photocurrent transients, and the electrochemical impedance spectra. The results indicated that target solid-state materials from liquid molten salts can be obtained ultimately through molecular design and adjustments of molecular structure, which can be used effectively in photoelectrical devices.

## Introduction

Dye-sensitized solar cells (DSSCs) are a low production cost and high-efficiency alternative to conventional inorganic photovoltaic solar cell.<sup>1</sup> The reported highest efficiency DSSCs are composed of dyes sensitized nanocrystalline porous TiO<sub>2</sub> films and volatile liquid-state electrolytes.<sup>2</sup> However, the liquid electrolytes presented in such system have the series issues of leakage, evaporation, contamination of the solvents that hinder the progress of actual application.<sup>3</sup>

Solid semiconductor materials to collect positive charges can circumvent the above problems created by the liquid-electrolyte.<sup>4</sup> Hence, organic/inorganic solid-state semicon-

ductor materials, such as inorganic p-type semiconductors, organic conducting materials, are chosen to assemble all-solid-state DSSCs.<sup>5</sup> Inorganic p-type materials have been identified as one kind of effective solid electrolytes and a 3.8% high conversion efficiency ( $\eta$ ) was obtained in solid-state DSSCs.<sup>6</sup> However, inorganic p-type material derived all-solid-state DSSCs shows no stability. This should be ascribed to inorganic p-type materials tending to be oxidized under continuous illumination and the worsening of the interfacial contact between dye-sensitized TiO<sub>2</sub> and electrolyte along with the growth of age.<sup>7</sup> Another weakness of the inorganic materials is the decided chemical structure, resulting in the limitedly adjustable chemical/physical properties in the application of solid-state electrolytes.

Another substitute to liquid electrolyte is employing small-molecule-organic conducting material.<sup>8</sup> However, although a high 5%  $\eta$  was achieved by OMeTAD-based solid-state

\* To whom correspondence should be addressed. E-mail: zhajin@iccas.ac.cn.

<sup>†</sup> Beijing National Laboratory for Molecular Sciences.

<sup>‡</sup> Graduate University of the Chinese Academy of Sciences.

- (1) (a) O'Regan, B.; Grätzel, M. *Nature* **1991**, *353*, 737. (b) Kim, I. D.; Hong, J. M.; Lee, B. H.; Kim, D. Y.; Jeon, E. K.; Choi, D. K.; Yang, D. *J. App. Phys. Lett.* **2007**, *91*, 163109. (c) Longo, C.; Nogueira, A. F.; De Paoli, M. A.; Cachet, H. *J. Phys. Chem. B* **2002**, *106*, 5925. (d) Peter, L. M.; Walker, A. B.; Boschloo, G.; Hagfeldt, A. *J. Phys. Chem. B* **2006**, *110*, 13694. (e) Stathatos, E.; Lianos, P.; Lavrencic-Stangar, U.; Orel, B. *Adv. Mater.* **2002**, *14*, 354. (f) Furube, A.; Katoh, R.; Hara, K.; Sato, T.; Murata, S.; Arakawa, H.; Tachiya, M. *J. Phys. Chem. B* **2005**, *109*, 16406. (g) Dürr, M.; Rosselli, S.; Yasuda, A.; Nelles, G. *J. Phys. Chem. B* **2006**, *110*, 21899. (h) Mor, G. K.; Shankar, K.; Paulose, M.; Varghese, O. K.; Grimes, C. A. *Nano Lett.* **2006**, *6*, 215. (i) Mor, G. K.; Shankar, K.; Paulose, M.; Varghese, O. K.; Grimes, C. A. *App. Phys. Lett.* **2007**, *91*, 152111.
- (2) Nazeeruddin, M. K.; Kay, A.; Rodicio, I.; Baker, R. H.; Müller, E.; Liska, P.; Vlachopoulos, N.; Grätzel, M. *J. Am. Chem. Soc.* **1993**, *115*, 6382.
- (3) Grätzel, M. *Inorg. Chem.* **2005**, *44*, 6841.
- (4) (a) Kroeze, J. E.; Hirata, N.; Schmidt-Mende, L.; Orizu, C.; Ogier, S. D.; Carr, K.; Grätzel, M.; Durrant, J. R. *Adv. Fun. Mater.* **2006**, *16*, 1832. (b) Gebeyehu, D.; C. Brabec, J.; Padinger, F.; Fromherz, T.; Spiekermann, S.; Vlachopoulos, N.; Kienberger, F.; Schindler, H.; Sariciftci, N. S. *Synth. Met.* **2001**, *121*, 1549. (c) Ikeda, N.; Miyasaka, T. *Chem. Commun.* **2005**, *14*, 1886. (d) Lowman, G. M.; Hammond, P. T. *Small* **2005**, *1*, 1070. (e) Yang, H.; Yu, C. Z.; Song, Q. L.; Xia, Y. Y.; Li, F. Y.; Chen, Z. G.; Li, X. G.; Yi, T.; Huang, C. H. *Chem. Mater.* **2006**, *18*, 5173.

- (5) (a) Kumara, G. R. A.; Konno, A.; Shiratsuchi, K.; Tsukahara, J.; Tennakone, K. *Chem. Mater.* **2002**, *14*, 954. (b) Tennakone, K.; Senadeera, G. K. R.; De Silva, D. B. R. A.; Kottegoda, I. R. M. *App. Phys. Lett.* **2000**, *77*, 2367. (c) Wang, Y. P.; Yang, K.; Kim, S. C.; Nagarajan, R.; Samuelson, L. A.; Kumar, J. *Chem. Mater.* **2006**, *18*, 4215.

- (6) (a) Meng, Q. B.; Takahashi, K.; Zhang, X. T.; Sutanto, I.; Rao, T. N.; Sato, O.; Fujishima, A.; Watanabe, H.; Nakamori, T.; Urugami, M. *Langmuir* **2003**, *19*, 3572. (b) O'Regan, B.; Lenzmann, F.; Muis, R.; Wienke, J. *Chem. Mater.* **2002**, *14*, 5023. (c) Karlsson, P. G.; Bolik, Richter, S. J. H.; Mahrov, B.; Johansson, E. M. J.; Blomquist, J.; Uvdal, P.; Rensmo, H.; Siegbahn, H.; Sandell, A. *J. Chem. Phys.* **2004**, *120*, 11224.

- (7) Taguchi, T.; Zhang, X. T.; Sutanto, I.; Tokuhiko, K.; Rao, T. N.; Watanabe, H.; Nakamori, T.; Urugami, M.; Fujishima, A. *Chem. Commun.* **2003**, 2480.

- (8) (a) Bach, U.; Lupo, D.; Comte, P.; Moser, J. E.; Weissörtel, F.; Salbeck, J.; Spreitzer, H.; Grätzel, M. *Nature* **1998**, *395*, 583. (b) Johansson, E. M. J.; Karlsson, P. G.; Hedlund, M.; Ryan, D.; Siegbahn, H.; Rensmo, H. *Chem. Mater.* **2007**, *19*, 2071. (c) Zhao, Y.; Chen, W.; Zhai, J.; Sheng, X. L.; He, Q. G.; Wei, T. X.; Bai, F. L.; Jiang, L.; Zhu, D. B. *Chem. Phys. Lett.* **2007**, *445*, 259.

DSSCs,<sup>9</sup> there are no satisfied and stable efficiencies compared with those using liquid-phase electrolytes. Therefore, exploring new electrolyte material with excellent physical/chemical properties and derived high photoelectrical performance is very important for the real applications of DSSCs.

Stemming from their large electrochemical window, high charge conductivity, negligible vapor pressure, and nontoxicity, ionic liquids (IL) as solvents have been a hot topic of extensive studies in DSSCs.<sup>10</sup> Among them, imidazolium-based compounds have been the most popular materials as electrolytes because of their emerged high performance in DSSCs.<sup>11</sup> However, they are still a type of liquid materials. Here, we modified the molecular structure of ionic liquid to synthesize a small-molecule-organic ionic crystal material, 1-methyl-3-acetyl-imidazolium iodide (MA-II). All-solid-state DSSCs was constructed using MA-II as a charge transfer layer, and the highest total conversion efficiencies of 2.6 and 2.0% were obtained at 1/2 and 1 simulated solar light (AM1.5) after incorporating functional additives, respectively. The photovoltage and photocurrent transients and the electrochemical impedance spectra were employed to investigate the inner operating mechanism of DSSCs. The new organic ionic compound based on molecular design will broaden our eyeshot to find a series of new electrolyte materials with potential high photoelectrical characters in the application of solvent-free DSSCs.

## Experimental Section

**Sample Preparation.** Organic ionic crystal, 1-methyl-3-acetyl-imidazolium iodide (MA-II), was synthesized by quaternization reactions of 1-methylimidazole with an equimolar amount of the iodoacetic acid for 72 h under a N<sub>2</sub> atmosphere at 70 °C. A representative procedure for the synthesis of MA-II is given below. 1-Methylimidazole with an equimolar amount of the iodoacetic acid was injected into an oven-dried, vacuum-cooled round-bottomed flask. The flask was fitted with a condenser and allowed to reflux for 72 h in acetonitrile. It was then cooled under 0 °C. The top liquid phase, containing unreacted starting reactants, was decanted and discarded. The bottom white solid was washed three times with *n*-hexane and acetonitrile in turn to remove any remaining unreacted reagents. Residual organic solvents were removed by heating the bottom phase (60 °C) under vacuum (12 h), producing a white solid. The crystallized product was finally confirmed by <sup>1</sup>H NMR in D<sub>2</sub>O and FT-IR. MA-II: mp: 188–189 °C;  $\sigma = 1 \times 10^{-5}$  S/cm; <sup>1</sup>H NMR (D<sub>2</sub>O,  $\delta$ /ppm relative to TMS): 3.97 (s, 3H), 4.98 (s, 2H), 7.50 (2H), 8.78 (s, 1H). The solid electrolyte was prepared by dissolving MA-II (0.32 g, 1.2 mmol), I<sub>2</sub> (0.06 g, 0.24 mmol), MP-BF<sub>4</sub> (0.025 g, 0.12 mmol), Li[(CF<sub>3</sub>SO<sub>2</sub>)<sub>2</sub>N] (0.07 g, 0.24 mmol), *t*BP (0.08 g, 0.06 mmol) into 10 mL ethanol.

**Photoelectrochemical Solar Cells.** Dye-sensitized photovoltaic solar cells were fabricated as previously described [8c]. TiO<sub>2</sub>

electrode was prepared as follows: Conductive fluorine-doped tin oxide (FTO) glass slides (Asahi, 30  $\Omega/\square$ ) were cleaned in a solution of detergent in water; rinsed with distilled water, acetone, and ethanol in turn; and dried in a nitrogen stream. A dense TiO<sub>2</sub> thin layer was produced on the FTO glass to isolate the conducting glass surface from the solid-state electrolytes. The TiO<sub>2</sub>/polyvinylalcohol colloid solution was electrospayed onto the FTO substrate with the high voltage electrohydrodynamic equipment. The detailed experiments can be found elsewhere.<sup>12</sup> The films were annealed at 450 °C for 45 min in air, resulting in 10  $\mu$ m thick films. The as-prepared electrode was put into 0.2 M TiCl<sub>4</sub> aqueous solution overnight at room temperature and annealed again for 30 min at 450 °C in air. The dye, Ru(dcbpy)<sub>2</sub>(NCS)<sub>2</sub> (dcbpy=2,2'-bipyridine-4,4'-dicarboxylic acid) (N3, Solaronix) was adsorbed by immersing the electrodes for 24 h in an ethanol 0.3 mM solution of the dye. After drying the electrode, the solution of solid-state electrolyte was dropped repeatedly onto the porous photoanode placed on a hot plate with the temperature of 50 °C till the porous film was filled with solid-state electrolyte. The solid-state heterojunction was then covered by a platinized conducting glass as a counter electrode to form a sandwich solar cell device. The platinized conducting glass is prepared from vacuum deposition of Pt by a magnetron sputtering apparatus (SBC-12, KYKY).

**Measurements.** The conductivities of MA-II and MA-II/I<sub>2</sub> were determined by a four-electrode system. The melting point of MA-II was recorded by a melting-point apparatus with microscope. Photovoltaic performance of DSSCs was measured using an electrochemical analyzer (CHI630B, Chenhua Instruments Co., Shanghai) under 100 mW/cm<sup>2</sup> irradiation of solar simulator illumination (CMH-250, Aodite Photoelectronic Technology Ltd., Beijing), which was calibrated by standard crystalline silicon solar cell (the 18th Research Institute of Electronics Industry Ministry, China). The incident photon to current conversion efficiency (IPCE) curves of DSSCs were measured by illumination with monochromatic light, which was obtained by passing light through a series of light filters with different wavelengths. The surface morphology and thickness of these TiO<sub>2</sub> films and dye sensitized heterojunction were determined by a scanning electron microscope (SEM) (JEOL, JSM-6700F). The electrochemical impedance measurements were carried out on a Zahner IM6eX impedance analyzer (Germany) in the frequency range from 0.02 Hz to 100 KHz under illumination of 100 mW/cm<sup>2</sup> and open-circuit condition. A GCR-4 Nd: YAG laser (Spectra Physics) ( $\lambda = 532$  nm, laser pulse width = 6 ns) was employed for transient photovoltage and photocurrent measurements. A TDS3032 oscilloscope (Tektronix) was used for recording transient photovoltage and photocurrent generation. The pulse spot size and thickness of TiO<sub>2</sub> film are 0.2 cm<sup>2</sup> and 10  $\mu$ m, respectively.

## Results and Discussion

**Synthesis and Characterization of MA-II.** As known, one of the most outstanding characters for small-molecule-organic materials is their infinitely adjustable molecular structure, which can be used to alter the physical/chemical properties of the compound. Considering that the imidazolium-based ionic liquids are a kind of high-performance electrolytes in DSSCs, an acetyl group was introduced into the imidazolium-type ionic conductor to form MA-II in this case. MA-II was synthesized by quaternization reactions of 1-methylimidazole with an equimolar amount of the iodoacetic

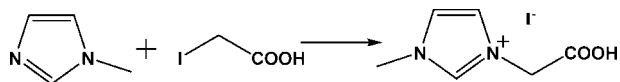
(9) Snaith, H. J.; Moule, A. J.; Klein, C.; Meerholz, K.; Friend, R. H.; Grätzel, M. *Nano Lett.* **2007**, *7*, 3372.

(10) Dupont, J.; de Souza, R. F.; Suarez, P. A. Z. *Chem. Rev.* **2002**, *102*, 3667.

(11) (a) Wang, P.; Zakeeruddin, S. M.; Moser, J. E.; Humphry-Baker, R.; Grätzel, M. *J. Am. Chem. Soc.* **2004**, *126*, 7164. (b) Mohmeyer, N.; Kuang, D. B.; Wang, P.; Schmidt, H. W.; Zakeeruddin, S. M.; Grätzel, M. *J. Mater. Chem.* **2006**, *16*, 2978. (c) Chen, D.; Zhang, Q.; Wang, G.; Zhang, H.; Li, J. H. *Electrochem. Commun.* **2007**, *9*, 2755. (d) Chen, Z. G.; Li, F. Y.; Yang, H.; Yi, T.; Huang, C. H. *ChemPhysChem* **2007**, *8*, 1293.

(12) (a) Zhao, Y.; Sheng, X. L.; Zhai, J.; Jiang, L.; Yang, C. H.; Sun, Z. W.; Li, Y. F.; Zhu, D. B. *ChemPhysChem* **2007**, *8*, 856. (b) Zhao, Y.; Zhai, J.; Tan, S.; Wang, L.; Jiang, L.; Zhu, D. B. *Nanotechnology* **2006**, *17*, 2090.

## Scheme 1. Synthesis of MA-II



tic acid as shown in Scheme 1. The crystallized products were washed with organic solvent and dried under a vacuum. The molecular structure was confirmed by  $^1\text{H}$  NMR in  $\text{D}_2\text{O}$  and FT-IR.  $^1\text{H}$  NMR ( $\text{D}_2\text{O}$ ,  $\delta/\text{ppm}$  relative to TMS): 3.97 (s, 3H), 4.98 (s, 2H), 7.50 (2H), 8.78 (s, 1H). The detailed synthetic procedure can be found in experimental section. Figure 1 shows the photograph of MA-II, indicating that the synthesized MA-II is white solid powder at room temperature. The acetyl group of molecules produced strong intermolecular hydrogen bonds. This strong intermolecular interaction resulted in the phase transformation from liquid-state of ionic liquids to solid-state crystals. The melting point of MA-II was increased to 188–189 °C. In addition, the adjustment of molecular structure also changed the ionic conductivity of materials. The conductivity of MA-II is  $1 \times 10^{-5}$  S/cm ( $\sigma = 1 \times 10^{-5}$  S/cm), which is a little lower than those of ionic liquids. After a quantity of iodine ( $n(\text{MA-II}):n(\text{I}_2) = 5:1$ ) was added, the conductivity was improved to  $3.8 \times 10^{-5}$  S/cm.

**Film Morphology.** Figure 2a shows the scanning electron microscope (SEM) photograph of the dye-sensitized  $\text{TiO}_2$  thin film prepared by electro-spray technique, exhibiting the hierarchical porous structures with enhanced roughness.<sup>12</sup> After depositing MA-II/ $\text{I}_2$  electrolyte into the sensitized  $\text{TiO}_2$  porous films, the largely and perfectly shaped MA-II crystals can be seen clearly in a large area (Figure 2b). It is due to the crystallization of small molecules. The sizes of crystals are about 1 to 5  $\mu\text{m}$  and the crystal layer has covered on  $\text{TiO}_2$  surface. As we know, ionic crystallization greatly prevents the filling of solid-state electrolyte into the  $\text{TiO}_2$  porous structure, resulting in a big decrease in photoelectrical characters of devices. So a crystal growth inhibitor, 1-methyl-3-propyl-imidazolium tetra-fluoroborate (MP-BF<sub>4</sub>), was introduced into solid electrolyte. Figure 2c shows the SEM images of MA-II/ $\text{I}_2$  electrolyte deposited into the sensitized  $\text{TiO}_2$  porous film in the presence of MP-BF<sub>4</sub>. A smooth surface morphology of dye-sensitized heterojunction can be clearly found. Figure 2d shows the side view of dye sensitized heterojunction. (The magnified side view is given in the Supporting Information, Figure S1) The  $\text{TiO}_2$  porous film network is completely filled by MA-II/ $\text{I}_2$  in the presence of MP-BF<sub>4</sub> with almost no voids, inhibiting the view of the porous  $\text{TiO}_2$  network. Based on the thickness of the  $\text{TiO}_2$  film measured before filling, a small amount of the composite electrolyte exists as an overlayer coating. Hence, an excellent

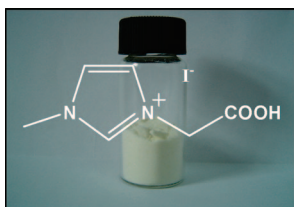


**Figure 1.** Molecular structure and photograph of 1-methyl-3-acetyl-imidazolium iodide (MA-II).

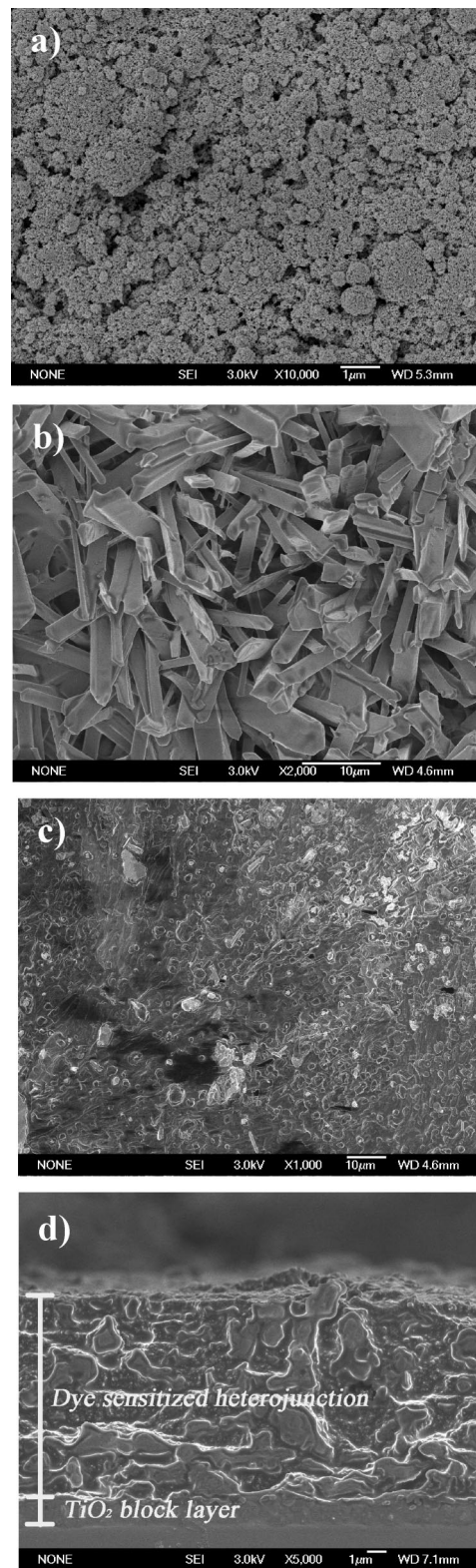


**Figure 2.** (a) SEM photograph of  $\text{TiO}_2$  hierarchical composite photoanode; (b) SEM photograph of MA-II/ $\text{I}_2$  layer deposited on the dye sensitized  $\text{TiO}_2$  porous film without molten salt in the solution; (c) SEM photograph of MA-II/ $\text{I}_2$  layer on the dye sensitized  $\text{TiO}_2$  porous film with molten salts in the solution.

interfacial contact between the dye-sensitized  $\text{TiO}_2$  and solid-state electrolytes was achieved.

**Photoelectrical Properties of All-Solid-State DSSCs.** The photocurrent density–voltage curves for the DSSCs with MA-II electrolyte containing molten salt MP-BF<sub>4</sub> (device 1),

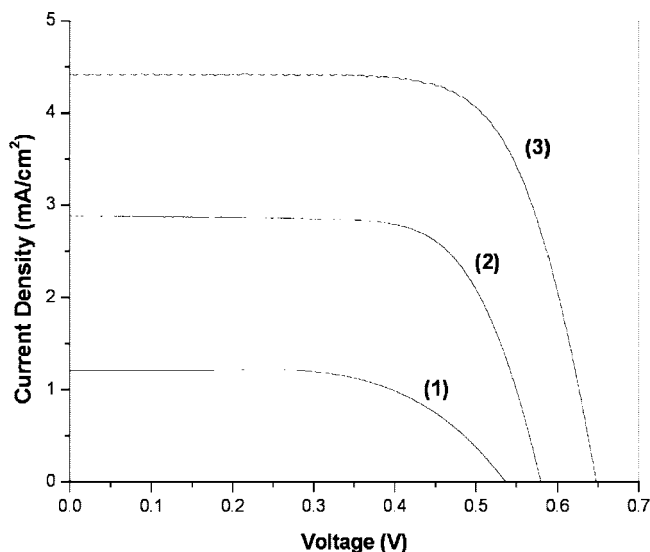


**Figure 3.** Photocurrent density–voltage characteristics of DSSCs with (1) MA-II based electrolyte added with MP-BF<sub>4</sub>; (2) MA-II based electrolyte added with MP-BF<sub>4</sub> and Li[(CF<sub>3</sub>SO<sub>2</sub>)<sub>2</sub>N]; (3) MA-II based electrolyte added with MP-BF<sub>4</sub>, Li[(CF<sub>3</sub>SO<sub>2</sub>)<sub>2</sub>N] and *t*BP. The sensitizer was N3 (Ruthenium dye). The cell active area was 0.2 cm<sup>2</sup> and the light intensity was 100 mW cm<sup>-2</sup>. Five devices for every type of photoanode were tested, and the average data are shown here.

**Table 1. Photoelectrical Parameters of DSSCs with MA-II Electrolyte-Based Electrolytes Doped with Different Additives**

electrolyte <sup>a</sup>	$J_{sc}$ (mA/cm <sup>2</sup> )	$V_{oc}$ (V)	$ff$ (%)	$\eta$ (%)
MA-II/I <sub>2</sub>	0.8	0.528	47	0.20
MA-II/I <sub>2</sub> +1 (device 1)	1.21	0.538	62	0.40
MA-II/I <sub>2</sub> +1 + 2 (device 2)	2.88	0.581	69	1.20
MA-II/I <sub>2</sub> +1 + 2+3 (device 3)	4.42	0.647	71	2.00

<sup>a</sup> MA-II, 1-methyl-3-acetyl-imidazolium iodide; 1, MP-BF<sub>4</sub>; 2, Li[(CF<sub>3</sub>SO<sub>2</sub>)<sub>2</sub>N]; 3, *t*BP.

that with MA-II electrolyte containing MP-BF<sub>4</sub> and Li[(CF<sub>3</sub>SO<sub>2</sub>)<sub>2</sub>N] (device 2), and the device with MA-II electrolyte containing MP-BF<sub>4</sub>, Li[(CF<sub>3</sub>SO<sub>2</sub>)<sub>2</sub>N] and *tert*-butylpyridine (*t*BP) (device 3) are presented in Figure 3 at an AM 1.5 irradiance of 100 mW cm<sup>-2</sup>. The photoelectrical parameters of DSSCs with different electrolytes are also listed in Table 1. Five solar devices for each kind of electrolytes were detected, and the data shown here were the average values. The deviations of  $\eta$  values do not exceed 10% of the averages. The open-circuit voltage ( $V_{oc}$ ), short-circuit current density ( $J_{sc}$ ), and fill factor ( $ff$ ) of DSSCs without any additives in its electrolyte are 528 mV, 0.8 mA cm<sup>-2</sup>, and 47%, respectively, yielding an overall power conversion efficiency ( $\eta$ ) of 0.2%. For device 1 with 1/10 molar quantity molten salt, the corresponding device parameters ( $V_{oc}$ ,  $J_{sc}$ ,  $ff$ , and  $\eta$ ) are increased to 1.21 mA cm<sup>-2</sup>, 538 mV, 62%, and 0.4%, respectively. The MA-II crystals of large sizes make many interspaces in the film and incomplete penetration of electrolyte into the porous network structure. Therefore, the bad electrical contact between the TiO<sub>2</sub> porous surface and the electrolytes is formed. The poor interfacial contact decreases the efficiency of holes injection from the sensitizer molecules into solid electrolytes dramatically, and then lowers the conversion efficiency of DSSC. In this case, addition of molten salt reduces direct contact between the MA-II crystals and the naked TiO<sub>2</sub> film and

thus lowers the charge combination probability between them. It also improves the interfacial wetting properties and reduces deterioration of the MA-II itself, and then the lifetime of the solar cell is enhanced. Device 2 shows a  $J_{sc}$  of 2.88 mA/cm<sup>2</sup>, a  $V_{oc}$  of 581 mV, a  $ff$  of 69%, and the  $\eta$  is improved to 1.2%. There is about a 185% increase in conversion efficiency compared to those without lithium salt. Here, the addition of lithium bis-trifluoro-methanesulfonylimide (Li[(CF<sub>3</sub>SO<sub>2</sub>)<sub>2</sub>N]) can improve the capability of charge transport and inhibit charge recombination, and then benefit for photovoltaic performance. The best photoelectrical performance of DSSCs was revealed in device 3. The corresponding parameters ( $V_{oc}$ ,  $J_{sc}$ ,  $ff$ , and  $\eta$ ) are 4.42 mA cm<sup>-2</sup>, 647 mV, 71%, and 2.0%, respectively. The  $\eta$  was enhanced about 10 times compared to the devices without any dopants. The key photoelectrical parameters, fill factor, was improved gradually after introducing the functional molecules, from 47 to 62% after doping MP-BF<sub>4</sub>, from 62 to 69% after continuously adding Li[(CF<sub>3</sub>SO<sub>2</sub>)<sub>2</sub>N], and to the highest value of 71% after incorporating all three additives. It indicated that the functional molecules take significant roles in photovoltaic performance of devices. Beside these devices, solid-state DSSCs with MA-II/I<sub>2</sub>, MP-BF<sub>4</sub>, and *t*BP were also fabricated. The conversion efficiency achieved to 0.9% ( $V_{oc}$  = 0.633 V,  $J_{sc}$  = 1.96 mA/cm<sup>2</sup>,  $ff$  = 75%), which is higher than that of device without *t*BP (see the Supporting Information, Figure S2 and Table S1) It indicated that the positive effect can be found in the enhancement of  $V_{oc}$  and  $J_{sc}$ . In addition, the overall conversion efficiency of devices 1, 2, and 3 were 0.52, 1.46, and 2.6%, respectively, under the light intensity illumination of 50 mW cm<sup>-2</sup>. (see the Supporting Information, Table S2) The discrepancy of the photovoltaic performance between 1 sun and 1/2 sun was due to the nonlinear behavior of photocurrent at higher light intensity. In the solid-state electrolyte, the photocurrent loss observed under full sunlight illumination is caused by carriers transport limitation due to the solid state of the electrolyte.<sup>13</sup> The photocurrent action spectrum of devices 3 sensitized with the dye N3 is given in Figure 4. The spectrum is close to the absorption spectra of the sensitizer, indicating that the generated photocurrent results from electron injection of the dye. The maximum incident monochromatic phototo-current conversion efficiency is ca. 34% at 530 nm for DSSCs with MA-II/I<sub>2</sub> electrolytes containing MP-BF<sub>4</sub>, Li[(CF<sub>3</sub>SO<sub>2</sub>)<sub>2</sub>N] and *t*BP. It demonstrates that MA-II based solid-state DSSCs have good photogenerated current density.

**Measurements of the Photovoltage and Photocurrent Transients.** In order to better elucidate charge transport and recombination in the inner of DSSCs, the transients photovoltage and photocurrent spectra of the devices with and without Li[(CF<sub>3</sub>SO<sub>2</sub>)<sub>2</sub>N] and *t*BP were measured (Figure 5). When the dye was excited by solar photons, the photocurrent and photovoltage responses in all of the DSSCs instantaneously reached maxima. The peak value of device 3 is the highest, while the smallest value is from device 1. It indicated

(13) Kuang, D. B.; Walter, P.; Nuesch, F.; Kim, S.; Ko, J.; Comte, P.; Zakeeruddin, S. M.; Nazeeruddin, M. K.; Grätzel, M. *Langmuir* **2007**, *23*, 10906.

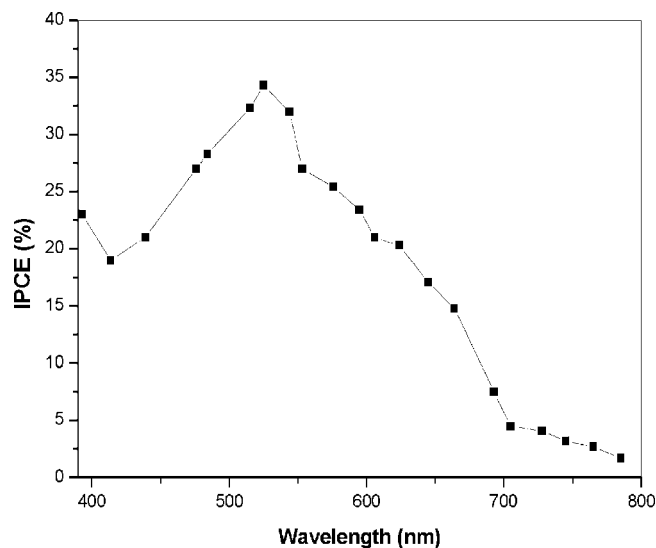


Figure 4. Photocurrent action spectra of MA-II electrolyte-based device 3 with MP-BF<sub>4</sub>, Li[(CF<sub>3</sub>SO<sub>2</sub>)<sub>2</sub>N] and tBP.

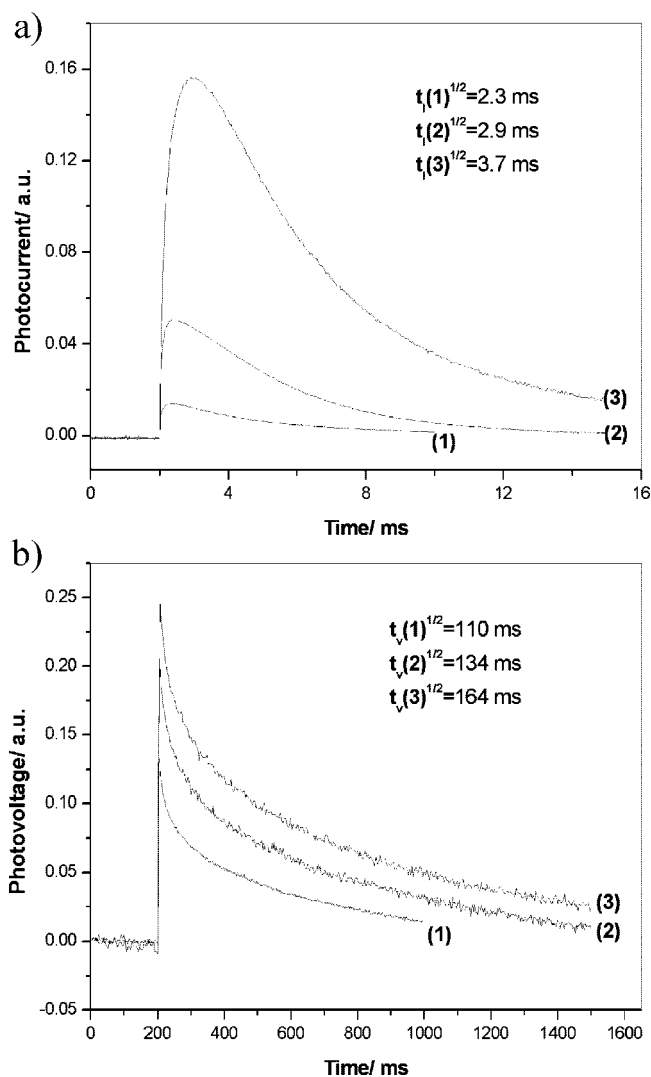
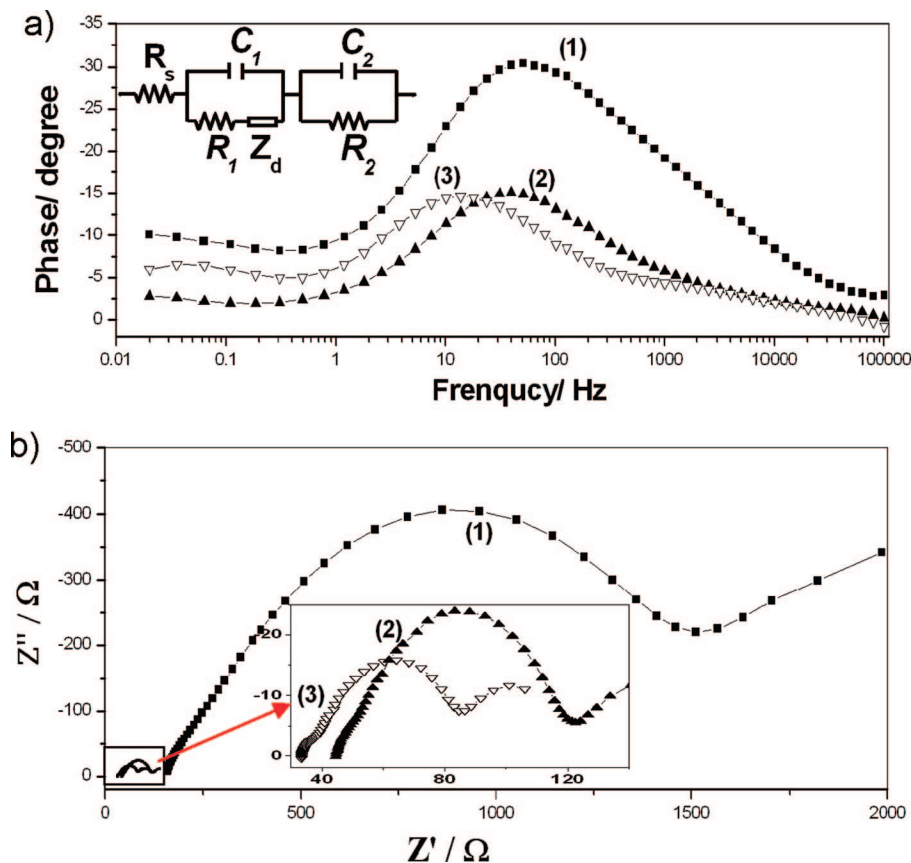


Figure 5. (a) Photocurrent and (b) photovoltage transients of the solid-state DSSCs devices 1, 2, and 3 with MA-II based electrolyte.

that DSSCs in presence of lithium salt and tBP could generate the highest photocurrent under the same light illumination and active areas. In addition, the decay rates of different

devices are different. In order to analyze spectrum and avoid unnecessary complexity, a transit time,  $t^{1/2}$ , which is defined and discussed as the time when the photovoltage or photocurrent decays to half of the peak value, is introduced in our discussion. For device 1,  $t_v(1)^{1/2} = 110$  ms and  $t_i(1)^{1/2} = 2.3$  ms (here  $t_v^{1/2}$  and  $t_i^{1/2}$  are referred as  $t^{1/2}$  in the photovoltage and photocurrent transients, respectively). For device 2, the obtained  $t_v(2)^{1/2}$  and  $t_i(2)^{1/2}$  is 134 and 2.9 ms, respectively. The  $t_v(2)^{1/2}$  and  $t_i(2)^{1/2}$  increase about 22 and 26% compared to those without Li[(CF<sub>3</sub>SO<sub>2</sub>)<sub>2</sub>N]. After incorporating Li[(CF<sub>3</sub>SO<sub>2</sub>)<sub>2</sub>N] and tBP into solid-state electrolyte, the  $t_v(3)^{1/2}$  and  $t_i(3)^{1/2}$  of Device 3 are improved to 164 and 3.7 ms, respectively. The corresponding parameters ( $t_v^{1/2}$  and  $t_i^{1/2}$ ) increase about 50 and 61% compared to those in the absence of Li[(CF<sub>3</sub>SO<sub>2</sub>)<sub>2</sub>N] and tBP. The positive effects of lithium ions and tBP on the photoelectrical characters of liquid DSSCs are comprehensively investigated.<sup>14</sup> Because both of the dye regeneration rate by I<sup>-</sup> and the rereduction rate of I<sup>-</sup> by electrons from the external circuit is much quicker than the charge recombination rate between the injected photoelectrons and oxidized dye/I<sub>3</sub><sup>-</sup>; in addition, both the mobile carriers and the negative charges of the redox couple I<sup>-</sup>/I<sub>3</sub><sup>-</sup> can screen photoelectrons and holes from each other in a liquid electrolyte and inhibit the recombination of I<sub>3</sub><sup>-</sup> with photoelectrons.<sup>15</sup> Therefore, the interfacial recombination can be neglected in the liquid DSSCs and the effect of lithium ions and tBP on the interfacial recombination is very limited. In liquid DSSCs, the positive effects of lithium ions and tBP on the photoelectrical performance is due to the fact that they can shift the conduction band/trap state of TiO<sub>2</sub> away from the vacuum level and promote the interfacial electron transfer to be energetically more favorable, and also they can suppresses the dark current at the TiO<sub>2</sub>/electrolyte junction, and so on.<sup>16</sup> Different from liquid DSSC, in solid-state devices, photogenerated carrier loss is mainly from the interfacial charge recombination.<sup>17</sup> This is ascribed to that the space charge layer is formed at the TiO<sub>2</sub>/electrolyte interface due to photoinduced charge injection, while the space charge layer is confined to a very thin layer because of the slower carriers transport of solid-state electrolyte. Ultimately, they cause photogenerated hole/electrons recombination.<sup>18</sup> The increase of  $t_v^{1/2}$  indicates that Li[(CF<sub>3</sub>SO<sub>2</sub>)<sub>2</sub>N] and tBP can alter the space charge layer and inhibit the interfacial hole/electron recombination. Meanwhile the increase of  $t_i^{1/2}$  is larger than that of  $t_v^{1/2}$ , which means that Li[(CF<sub>3</sub>SO<sub>2</sub>)<sub>2</sub>N] and tBP not

- (14) (a) Kelly, C. A.; Farzad, F.; Thompson, D. W.; Stipkala, J. M.; Meyer, G. J. *Langmuir* **1999**, *15*, 7047. (b) Haque, S. A.; Tachibana, Y.; Willis, R. L.; Moser, J. E.; Grätzel, M.; Klug, D. R.; Durrant, J. R. *J. Phys. Chem. B* **2000**, *104*, 538. (c) Schlichthörl, G.; Huang, S. Y.; Sprague, J.; Frank, A. J. *J. Phys. Chem. B* **1997**, *101*, 8141. (d) Olson, C. L. *J. Phys. Chem. B* **2006**, *110*, 9619.
- (15) (a) Gregg, B. A.; Pichot, F.; Ferrere, S. C.; Fields, L. J. *Phys. Chem. B* **2001**, *105*, 1422. (b) Schwarzburg, K.; Willig, F. *J. Phys. Chem. B* **1999**, *103*, 5743.
- (16) Huang, S. Y.; Schlichthörl, G.; Nozik, A. J.; Grätzel, M.; Frank, A. J. *J. Phys. Chem. B* **1997**, *101*, 2576.
- (17) Bach, U.; Krüger, J.; Grätzel, M. *Organic Photo Voltaics*; The International Society for Optical Engineering: San Diego, CA, 2000; Vol. 4108, p 1; (b) Xia, J. B.; Masaki, N.; Lira-Cantu, M.; Kim, Y.; Jiang, K. J.; Yanagida, S. *J. Am. Chem. Soc.* **2008**, *130*, 1258.
- (18) Krüger, J.; Plass, R.; Cevey, L.; Piccirelli, M.; Grätzel, M.; Bach, U. *Appl. Phys. Lett.* **2001**, *79*, 2085.



**Figure 6.** Electrical impedance spectra of device 1 ( $\square$ ), device 2 ( $\blacktriangle$ ), and device 3 ( $\blacksquare$ ) with MA-II based electrolyte in the forms of (a) Nyquist plots and (b) Bode plots. (The insets of a and b are the equivalent circuit of devices.) The spectra were measured under an illumination of 1 sun at open-circuit potential.

only lower the interfacial charge recombination, but also improve charge transport of MA-II-based electrolytes.<sup>19</sup> The addition of  $\text{Li}^+$  and tBP can optimize the space charge layer, shift the conduction band of  $\text{TiO}_2$  to higher energies and improve the charge transport ability, resulting in the improvement of  $V_{oc}$  and  $J_{sc}$ . The inhibited charge recombination was also testified by the measurements of dark  $I-V$  characteristic (see the Supporting Information, Figure S3).

**Electrochemical Impedance Measurements of Solid-State DSSCs.** For the inner work process of DSSCs, such as the essence of holes or ions transport processes and the behaviors of interfacial charge transport, can be understood by measuring the electrochemical impedance spectrum (EIS) of solar devices.<sup>20</sup> The data were collected under illumination of one sun at open-circuit potential and the EIS was shown in Figure 6. The figures are given in the form of Nyquist (top) and Bode (bottom) plots, respectively. In general, three characteristic arcs can be found in the Nyquist plots in the measurement of standard liquid DSSCs. The lowest-frequency semicircle is attributed to the Nernst diffusion of the redox within the electrolyte (ca. 0.01–1 Hz); the medium-frequency semicircle related to photoinjected electron transfer in the  $\text{TiO}_2$  or back reaction from the injected electrons in  $\text{TiO}_2$  to the electrolyte (ca. 1–100 Hz); the redox reactions

of the platinum counter electrode are revealed in the highest frequency semicircle (ca.  $10^0$ – $10^4$  Hz).<sup>21</sup> The equivalent circuit of this model (Inset of Figure 6a) has been already reported.<sup>22</sup> In the lowest frequency range, values of  $R_s$  (charge transport resistance of boundaries) for device 1, device 2, and device 3 are ca. 157, 44, and 33  $\Omega$ , respectively. This indicates that introducing  $\text{Li}[(\text{CF}_3\text{SO}_2)_2\text{N}]$  and tBP reduces charge transport resistance of the interface of Pt counter electrode and solid-state electrolyte. Fitting the medium-frequency semicircle subsequently gives  $C_2$  (capacity) and  $R_2$  (resistance of charge transfer). Compared with device 1, device 2 has a bigger  $C_2$  (150  $\mu\text{F}$  vs 0.7  $\mu\text{F}$ ), but a smaller  $R_2$  (82  $\Omega$  vs 1600  $\Omega$ ), showing the largely depressed carriers recombination with  $\text{Li}[(\text{CF}_3\text{SO}_2)_2\text{N}]$  as an additive in electrolyte. Device 3 gives the biggest  $C_2$  (270  $\mu\text{F}$ ) and the smallest  $R_2$  (64  $\Omega$ ), indicating the lowest hole/electron recombination action among the three devices. From the medium-frequency semicircle in Bode, it can be seen that the medium frequency peak of device 2 is shifted to lower frequency compared to that of device 1, which was not doped with  $\text{Li}[(\text{CF}_3\text{SO}_2)_2\text{N}]$  into the electrolyte. In device 3, the medium frequency peak is shifted to the lowest frequency. It can be confirmed that the

(19) Nakade, S.; Saito, Y.; Kubo, W.; Kanzaki, T.; Kitamura, T.; Wada, Y.; Yanagida, S. *J. Phys. Chem. B* **2004**, *108*, 1628.

(20) Zhao, Y.; Zhai, J.; Wei, T. X.; Jiang, L.; Zhu, D. B. *J. Mater. Chem.* **2007**, *17*, 5084.

(21) Kuang, D. B.; Klein, C.; Zhang, Z. P.; Ito, S.; Moser, J. E.; Zakeeruddin, S. M.; Grätzel, M. *Small* **2007**, *3*, 2094.

(22) (a) Park, N. G.; Kim, K. M.; Kang, M. G.; Ryu, K. S.; Chang, S. H.; Shin, Y. J. *Adv. Mater.* **2005**, *17*, 2349. (b) Wang, Q.; Moser, J. E.; Grätzel, M. *J. Phys. Chem. B* **2005**, *109*, 14945. (c) van de Lagemaat, J.; Park, N. G.; Frank, A. J. *J. Phys. Chem. B* **2000**, *104*, 2044.

interfacial charge recombination between the photoinjected electron and electrolyte materials was encumbered, which has also been proved by the measurements of transient photovoltage and photocurrent mentioned above.<sup>23</sup> From the medium frequency of EIS Nyquist plots, it can be seen that the inner transport resistance of MA-II electrolyte without Li[(CF<sub>3</sub>SO<sub>2</sub>)<sub>2</sub>N] in DSSCs can be reduced enormously by adding Li[(CF<sub>3</sub>SO<sub>2</sub>)<sub>2</sub>N]. This is ascribed to that addition of lithium ion can improve the conductivity of MA-II electrolyte, and then lower the charge transport resistance in the DSSCs. In the Nyquist plots, there are linear behaviors in the low frequency range, demonstrating that there is slowly ionic diffusion in the MA-II based solid-state electrolyte system even if doping the Li[(CF<sub>3</sub>SO<sub>2</sub>)<sub>2</sub>N]/tBP. It can be concluded that carrier transport in the solid-state electrolyte is mainly from ionic diffusion conduction.<sup>23</sup>

### Conclusion and Perspective

By adjusting the molecular structure of ionic liquid, we synthesized a new ionic crystal, MA-II, and applied it into all-solid-state DSSCs as electrolyte materials. Under 1/2 sun and 1 sun light intensity illumination, total conversion efficiencies of 2.6 and 2.0% were obtained, respectively. The three additives, MP-BF<sub>4</sub>, Li[(CF<sub>3</sub>SO<sub>2</sub>)<sub>2</sub>N], and tBP, were introduced into MA-II electrolyte and the positive effects on photoelectrical performance were shown in the system of DSSCs, which was testified by the measurements of photovoltage, photocurrent transients, and the electrochemical impedance spectra.

Because of the good photoelectrical performance and stability (see the Supporting Information, Figure S4) of solar devices based on MA-II molecules, we think that a series of new ionic compounds will be developed and used in DSSCs. As the conductivity of ionic crystal MA-II is  $1 \times 10^{-5}$  S/cm, there is large space to improve. For example, embedding

other functional groups –OH, –NH<sub>2</sub> into imidazolium-type ionic liquid molecules can produce weaker intermolecular hydrogen bonds than those of –COOH, which induce lower melting points and higher ionic conductivity. Improved ionic conductivity of solid materials will benefit transport of the photogenerated holes, resulting in the higher photoelectrical performance. On the basis of our hypothesis, a hydroxyl group was introduced into imidazolium-type molecule, and 1-methyl-3-hydroxyethyl-imidazolium iodide (MH-II) was synthesized and applied into solid-state DSSCs. The melting point of MH-II was decreased to 55–57 °C, and the conductivity of MA-II increased to  $7.8 \times 10^{-4}$  S/cm ( $\sigma = 7.8 \times 10^{-4}$  S/cm). The photoelectrical performance of solid-state DSSCs with MH-II as charge transport layer achieved to 3.6 and 3.1% under 1/2 sun and 1 sun irradiation, respectively (the detailed synthesis and photoelectrical performance can be found in the Supporting Information, Figure S5 and Table S3). It indicated that the obtained MH-II is also a good solid-state electrolyte in DSSCs. In addition to the imidazolium-type ionic liquids, the physical/chemical properties of other types of ionic liquids with high ionic conductivity can be tuned by molecular design, producing intermolecular interaction force to form solid conducting materials. Further research is underway in our group to synthesize other ionic crystals with different functional groups so as to investigate their photoelectrical properties and the influence of different functional groups on the ionic conductivity and their derived solar cell devices.

**Acknowledgment.** This work was supported by the National Natural Science Foundation of China (20573120, 20773142, 50533030), the National Research Fund for Fundamental Key Projects (2006CB806200, 2006CB932100 and 2007CB936403) and 863 project (2007AA032348).

**Supporting Information Available:** Additional figures and tables (PDF). This material is available free of charge via the Internet at <http://pubs.acs.org>.

CM800673X

(23) Kern, R.; Sastrawan, R.; Ferber, J.; Stangl, R.; Luther, J. *Electrochim. Acta* **2002**, *47*, 4213.